Journal of Advanced Research in Applied Sciences and Engineering Technology

Journal homepage:
https://semarakilmu.com.my/journals/index.php/applied_sciences_eng_tech/index
ISSN: 2462-1943

Experimental Investigation of Bio-Oil Droplet Impact on Liquid Pools Across Wide Temperature and Weber Number Ranges

Omer Khalid Shihab Ertobah[1], Khairil Faizi Mustafa[1,*], Khaled Ali Mohammad Al-attab[1]

[1] School of Mechanical Engineering, Tuanku Syed Sirajuddin Engineering Campus, 14300 Nibong Tebal, Penang, Malaysia

ARTICLE INFO

Article history:
Received 29 March 2026
Received in revised form 5 May 2026
Accepted 25 May 2026
Available online 10 June 2026

Keywords:

Droplet impact; bio-oil; liquid pool surface; Weber number; high-speed imaging; vapour explosion

ABSTRACT

Droplet impact on liquid pool surfaces is important in spray cooling, thermal management, and fuel-related applications. However, the combined effects of temperature, Weber number, and liquid configuration on bio-oil droplet impact dynamics remain insufficiently understood, particularly in relation to splashing, jet formation, and vapour explosion behaviour. This study investigates single-droplet impacts on liquid pool surfaces under controlled thermal and dynamic conditions for water-to-water, water-to-oil, and oil-to-water configurations. Distilled water and selected bio-oils, including olive oil, peanut oil, sunflower oil, and a waste-oil/olive-oil blend, were tested over a temperature range from room temperature to 290 °C and at Weber numbers between 172 and 1011. High-speed imaging was employed to capture the transient interfacial dynamics. The results show that Weber number and temperature are dominant parameters governing droplet deformation, jet formation, and instability development. As impact intensity increases, water-to-oil impacts produce greater spreading, crown formation, and jet development, with maximum jet height reaching $Hj/D_o \approx 9.13$ and crown height up to $12.3D_o$. In contrast, oil-to-water impacts remain stable and splash-free across all tested conditions, highlighting the stabilizing influence of viscosity and liquid configuration. At 290 °C, vapour explosion events were observed, indicating intensified thermofluid interactions and rapid vapour generation at the liquid interface. These findings provide a unified physical understanding of the coupled effects of inertia, temperature, and liquid properties on bio-oil droplet interactions, while offering useful guidance for improving stability, heat transfer control, and safety in high-temperature industrial and renewable-energy systems.

1. Introduction

The impact of a droplet on a liquid surface is a complex phenomenon that can result in a wide range of outcomes, including spreading, partial coalescence, rebounding, and splashing, depending on the droplet velocity, size, and fluid properties [1-4]. This process has attracted significant attention due to its relevance in many scientific and engineering applications, such as spray cooling, inkjet

* *Corresponding author.*
E-mail address: mekhairil@usm.my

https://doi.org/10.37934/araset.60.5.145169

printing, fire suppression, coating processes, and combustion systems [5,6]. Droplet impact events are commonly encountered in both natural and industrial environments; however, their dynamics remain challenging to predict due to the coupled effects of inertia, surface tension, viscosity, and interfacial interactions [7]. These factors govern the evolution of key features such as crater formation, crown development, and jet generation. Previous studies have investigated these mechanisms through experimental, numerical, and theoretical approaches, highlighting the complex interplay between fluid properties and impact conditions [8-10].

A particularly important area of research is the impact of droplets on liquid pool surfaces, especially under elevated temperature conditions. In such systems, additional phenomena may arise, including secondary jet formation, bubble entrapment, and vapor explosions, which significantly alter the impact dynamics [11,13]. For example, previous studies have identified distinct regimes such as crater–jet–bubble sequences and explosive boiling behaviour when water droplets interact with heated oil pools [14]. The interaction between water droplets and heated oil pools has been widely investigated, where vapor explosions are reported to occur when the oil temperature exceeds approximately 210 °C, with the timing strongly influenced by droplet size and Weber number [15-17]. Similar observations have been reported for peanut oil systems, where both temperature and droplet diameter play a key role in triggering vapor explosions [11].

These findings confirm that inertia and thermal effects are dominant factors governing droplet–liquid interactions. Despite these advances, most existing studies have focused primarily on water droplets, while the behaviour of bio-oil droplets with varying viscosities and physical properties has received limited attention. In particular, the combined effects of viscosity, surface tension, and density on impact dynamics in systems involving vegetable oils and waste oil mixtures remain insufficiently understood. To address this gap, the present study investigates the impact of single bio-oil droplets (olive oil, sunflower oil, peanut oil, waste oil, and distilled water) on shallow liquid pool surfaces over a wide range of temperatures (28–290 °C) and Weber numbers (172–1011). The analysis considers both classical impact features, such as crater depth, crown dynamics, and jet formation, as well as more complex phenomena including jet breakup and vapor explosion behaviour. The primary objective is to clarify the roles of temperature, inertia (Weber number), and fluid properties in governing droplet impact regimes and instability mechanisms in liquid–liquid systems.

2. Methodology

Figure 1 illustrates the main components of the experimental setup. The system consists of a droplet generator coupled with a syringe pump, a precision heating unit, and a high-speed imaging system with LED backlighting. These components collectively form the core instrumentation used to investigate droplet impact dynamics. The syringe pump, with a minimum flow rate of 0.1 mL/h, was used to generate single droplets with controlled size and release frequency. The droplets were released vertically and allowed to fall under gravity. Three release heights (Hg) were maintained between the syringe tip and the pool surface: 20 cm, 50 cm, and 80 cm. The impact velocity was determined using image processing techniques and validated using the theoretical free-fall relation given in **Eq.** (1):

$$V = \sqrt{2g(h - D_o)} \quad (1)$$

where (h) is the release height, (D_o) is the initial droplet diameter, and (g) is the gravitational acceleration. The resulting velocities were 1.98, 3.13, and 3.96 m/s.

The experimental reservoir (100 × 100 × 100 mm) was fabricated from high-temperature-resistant quartz glass and maintained a liquid depth between 35 and 50 mm, corresponding to a Weber number range of 172 to 1011. The working fluids included distilled water, olive oil, sunflower oil, peanut oil, and a mixture of oils (50% pure olive oil and 50% waste olive oil). Uniform illumination was achieved using a 1500 W LED light source with a diffuser to ensure high image clarity. A high-speed camera (OLYMPUS i-Speed) was used to capture the impact dynamics at a resolution of 800 × 800 pixels and a shutter speed of 2000 μs, with a trigger threshold of 50%. The droplet diameter was determined using image analysis by measuring the horizontal and vertical diameters. The equivalent droplet diameter was calculated using **Eq.** (2)[18]

$$D_o = (Dx^2 Dy)^{1/3} \quad (2)$$

where Dx is the horizontal diameter and Dy is the vertical droplet diameter, respectively [19]. The experiments were conducted using droplet sizes ranging from 2.6 to 3.2 mm.

The pool temperature was measured using thermocouples positioned near the liquid surface and controlled at three levels: 28 °C, 80 °C, and 290 °C. Image processing and calibration were performed using i-Speed Viewer and ImageJ software. The thermophysical properties of the liquids are listed in **Table 1**, while the experimental conditions are summarized in **Table 2**.

To characterize the impact dynamics, several dimensionless numbers were employed. The Weber number (We), Reynolds number (Re), Froude number (Fr), and Ohnesorge number (Oh) are defined in **Eqs.** (3) – (6), respectively:

$$We = \frac{\rho U^2 D_0}{\sigma} \quad (3)$$

$$Re = \frac{\rho V D_0}{\mu} \quad (4)$$

$$Fr = \frac{V^2}{g\, D_0} \tag{5}$$

$$Oh = \frac{\mu}{\rho\, \sigma\, D_0} \tag{6}$$

where ρ is the liquid density, U is the impact velocity, D_0 is the initial droplet diameter, μ is the dynamic viscosity, σ is the surface tension, and g is the gravitational acceleration.

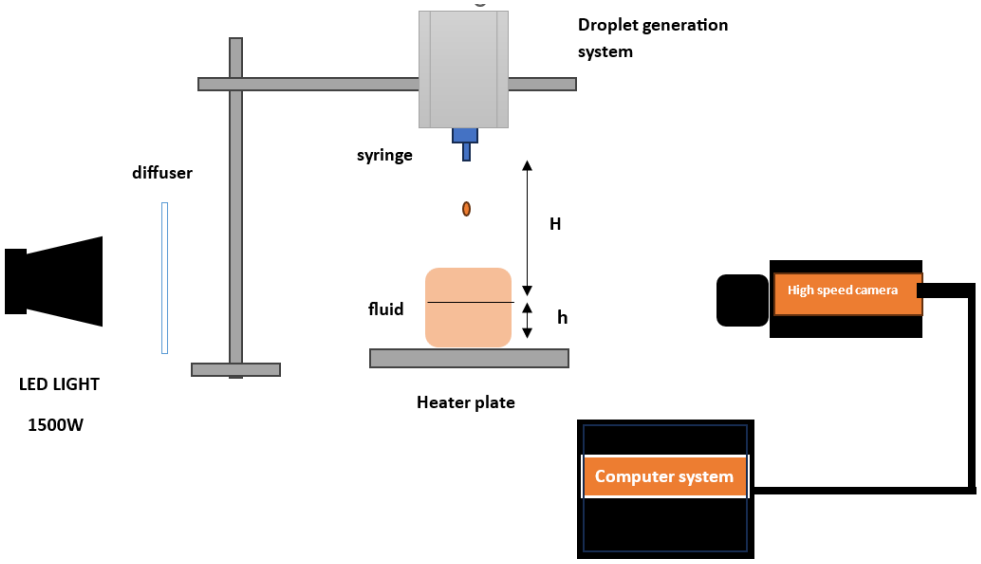

Fig. 1 Schematic representation of the experimental apparatus

Table 1
Physical properties at an ambient temperature of 28°C

Fluid	Density (kg/m3)	Surface tension N/M	Viscosity(cp)
Olive	0.8928	0.0383	43.79
Sunflower	0.8583	0.0360	34.32
Peanut	0.8274	0.0353	39.17
WCOO	0.8833	0.0356	40.4
Distilled water	0.9909	0.072	1

Table 2
Experimental conditions

Fluid	Height	D_o	V	Oh	Re	We	Fr
Olive oil		2.7mm		0.144	108-172-217	246-616-986	148-369-592
Peanut	20cm	2.6mm	1.98m/s	0.141	108-171-217	238-597-955	153-384-614
Sunflower	50cm	2.6mm	3.13m/s	0.121	128-203-257	243-607-972	153-384-614
WCOO	80cm	2.6mm	3.96m/s	0.141	112-177-225	252-632-1011	153-384-614
Distilled water		3.2mm		0.002	6278-9924-12556	172-431-690	11.17-17.66-22.35

3. Results

3.1 Droplet Impact on Pool Surfaces

The dynamic behaviour of a single droplet impacting a shallow pool surface is governed by the coupled interaction of inertia, viscosity, surface tension, temperature, and liquid–liquid asymmetry. In this study, the impact process was analyzed under three Weber number regimes (low, moderate, and high) and different thermal conditions (28 °C, 80 °C, and 290 °C) for three configurations: oil-to-water, water-to-oil, and water-to-water. Increasing Weber number progressively enhances droplet deformation, crater expansion, crown growth, and jet instability, while elevated temperature further modifies these regimes by reducing viscous resistance and promoting vapour generation. The impact process generally evolves through spreading, crater formation, crown development, and jet formation. Under high-temperature conditions, additional phenomena such as secondary jetting and vapour explosion are observed, indicating intensified thermofluid interactions at the liquid interface. The key geometric parameters used to characterize these processes are illustrated in **Figure 2**, including maximum crater depth (R_{max}), crater diameter (D_d), crown height (H_c), and jet height (H_j).

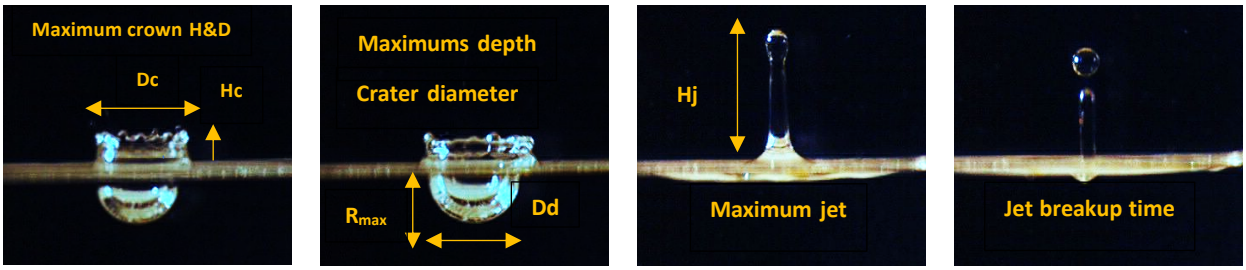

Fig. 2 Explore the impact of a single droplet on a constrained shallow pool surface

3.1.1 Oil-to-water droplet impact

At room temperature (28 °C), bio-oil droplets impacting a water pool exhibit smooth and stable behaviour across all Weber numbers, with no splashing observed. Following impact, the droplets penetrate the pool surface and undergo crater formation, crown development, and subsequent jet evolution. The absence of splashing suggests that viscous damping within the bio-oils, together with the cushioning effect of the water pool, effectively suppresses interfacial instability and rim breakup even at elevated Weber numbers. At low Weber numbers (We ≈ 238 – 252), droplet deformation is relatively mild, and inertial forces are insufficient to generate significant crown instability. The droplets penetrate smoothly and form shallow craters without visible crown formation ($H_c \approx 0$). The maximum crater depth is reached at approximately 29 ms, with values of $R_{max}/D_o \approx 2.32$ for olive oil, 2.50 for peanut oil, 2.41 for sunflower oil, and 2.27 for waste oil. Jet formation remains weak, with H_j/D_o ranging from approximately 2.0 to 3.7. Sunflower oil produces the highest jet due to its lower viscosity, whereas waste oil exhibits the most damped behaviour because a larger fraction of the impact energy is dissipated during crater collapse (**Figure 3**). As the Weber number increases to the moderate range (We ≈ 597 – 632), inertial effects become more pronounced, resulting in greater crater expansion, stronger jetting, and the onset of crown development. Maximum jet heights increase substantially, reaching $H_j/D_o \approx 6.52$ for olive oil, 8.15 for peanut oil, 8.43 for sunflower oil, and 6.96 for waste oil at approximately 42 – 46 ms. Crown formation also becomes more evident, with sunflower oil producing the highest crown height ($H_c \approx 2.71$), while waste oil exhibits the lowest value (Hc ≈ 1.85). These differences indicate that lower-viscosity oils transfer impact energy more efficiently into crater collapse and upward jet motion, whereas higher-viscosity oils limit deformation through enhanced viscous dissipation (**Figure 4**). At high Weber numbers (We ≈ 955–1011), inertial

effects become dominant, producing deeper craters, larger crowns, and stronger jet development. The maximum jet height occurs at approximately 49 ms, reaching $H_j/D_o \approx 8.57$ for sunflower oil, followed by peanut oil (7.71), waste oil (7.57), and olive oil (7.29). Crater diameters exceed $Dd/D_o > 5.7$, while crown heights increase up to $H_c \approx 5.17$ for olive oil. Despite these substantial deformations, no splashing occurs, confirming that viscous damping and liquid-pool cushioning continue to stabilize the interface even under high-inertia conditions (**Figure 5**). The variation of non-dimensional parameters with Weber number and time is further illustrated in **Figure 6**, where crater diameter, crown height, and jet height all increase progressively with Weber number. The temporal evolution of H_j/D_o also shows that increasing inertia delays crater collapse and shifts the occurrence of maximum jet formation from approximately 29 ms to 49 ms. Increasing the pool temperature to 80 °C does not fundamentally alter the impact behaviour, although the resulting deformation becomes noticeably more pronounced. At low Weber numbers, jet heights increase to approximately $H_j/D_o \approx 4.4 – 5.3$, accompanied by slightly larger crater widths (**Figure 7**). At moderate Weber numbers, crater diameters exceed $D_d/D_o \approx 5.3$ and jet heights reach approximately 8.7, while crown formation becomes increasingly evident compared with room-temperature conditions (**Figure 8**). At high Weber numbers, thermal effects become more significant (**Figure 9**). Maximum jet heights increase further to $H_j/D_o \approx 9.13$, while crown heights rise dramatically to $H_c \approx 7.51$, representing nearly a doubling relative to room temperature (**Figure 10**). This behaviour suggests that elevated temperature reduces viscous resistance and enhances interfacial mobility, thereby amplifying crater oscillation, crown growth, and jet instability. Overall, the oil-to-water system remains stable throughout the investigated Weber number and temperature ranges, with no splashing observed even under the most energetic conditions. The results indicate that bio-oil viscosity and liquid-pool cushioning play a dominant stabilizing role, suppressing instability growth while allowing larger crater deformation, crown expansion, and jet development as Weber number and temperature increase. Although higher inertia and temperature enhance the intensity of the impact, they do not fundamentally alter the stable nature of the oil-to-water interaction.

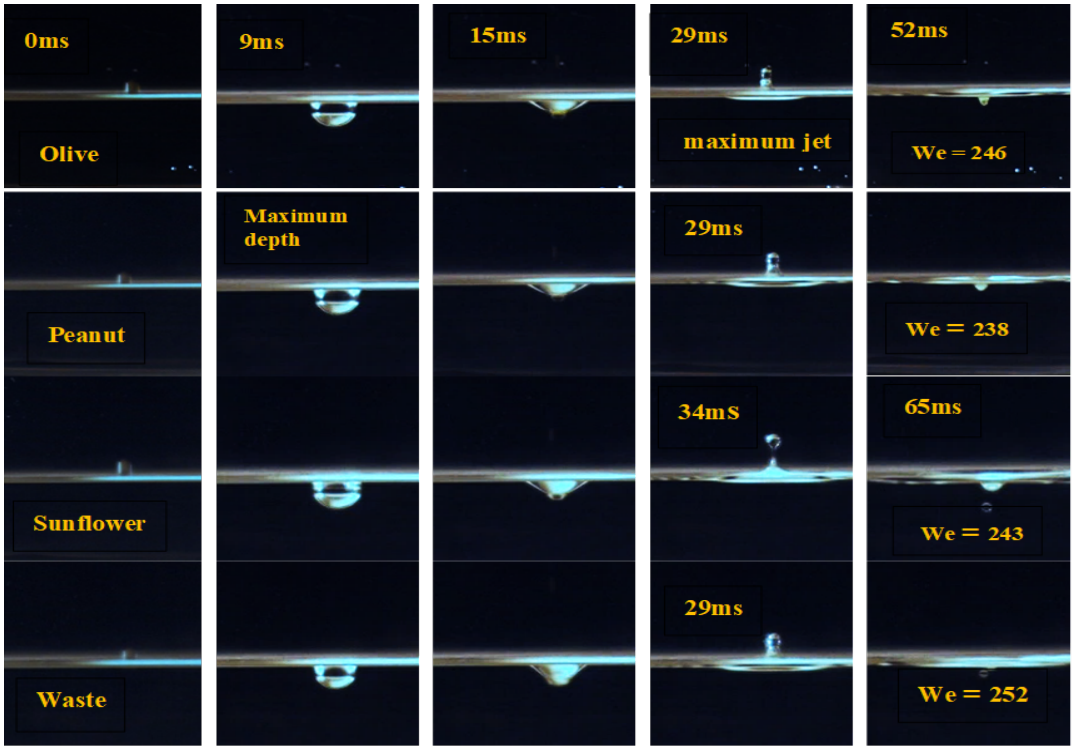

Fig. 3. Bio-oil single droplet on target distilled water pool surface under room temperature, with V=1.98 m/s, We from (238 to 252), and D initial = (2.6 to 2.7) mm

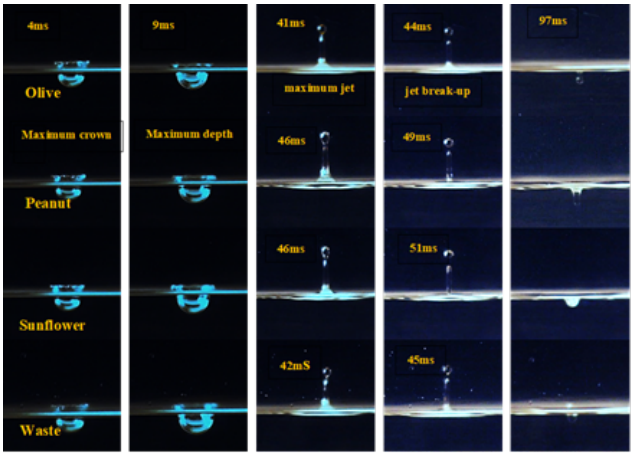

Fig. 4. Bio-oil single droplet on target distilled water pool surface under room temperature with V=3.13 m/s, We from (616 to 632) and D initial = (2.6 to 2.7)

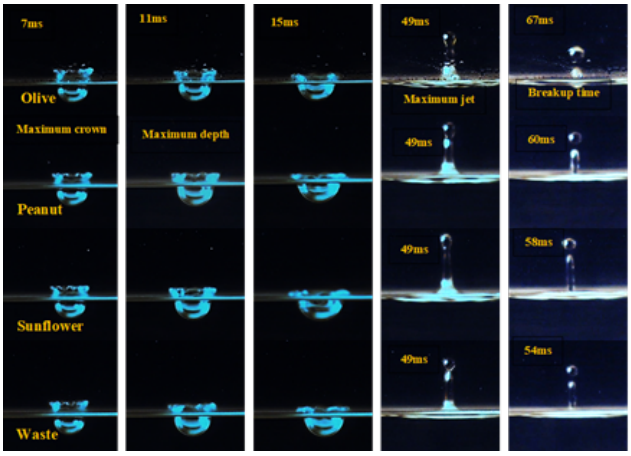

Fig. 5. Bio-oil single droplet on target distilled water pool surface under room temperature with V=3.96 m/s, We from (955 to 1011) and D initial = (2.6 to 2.7)

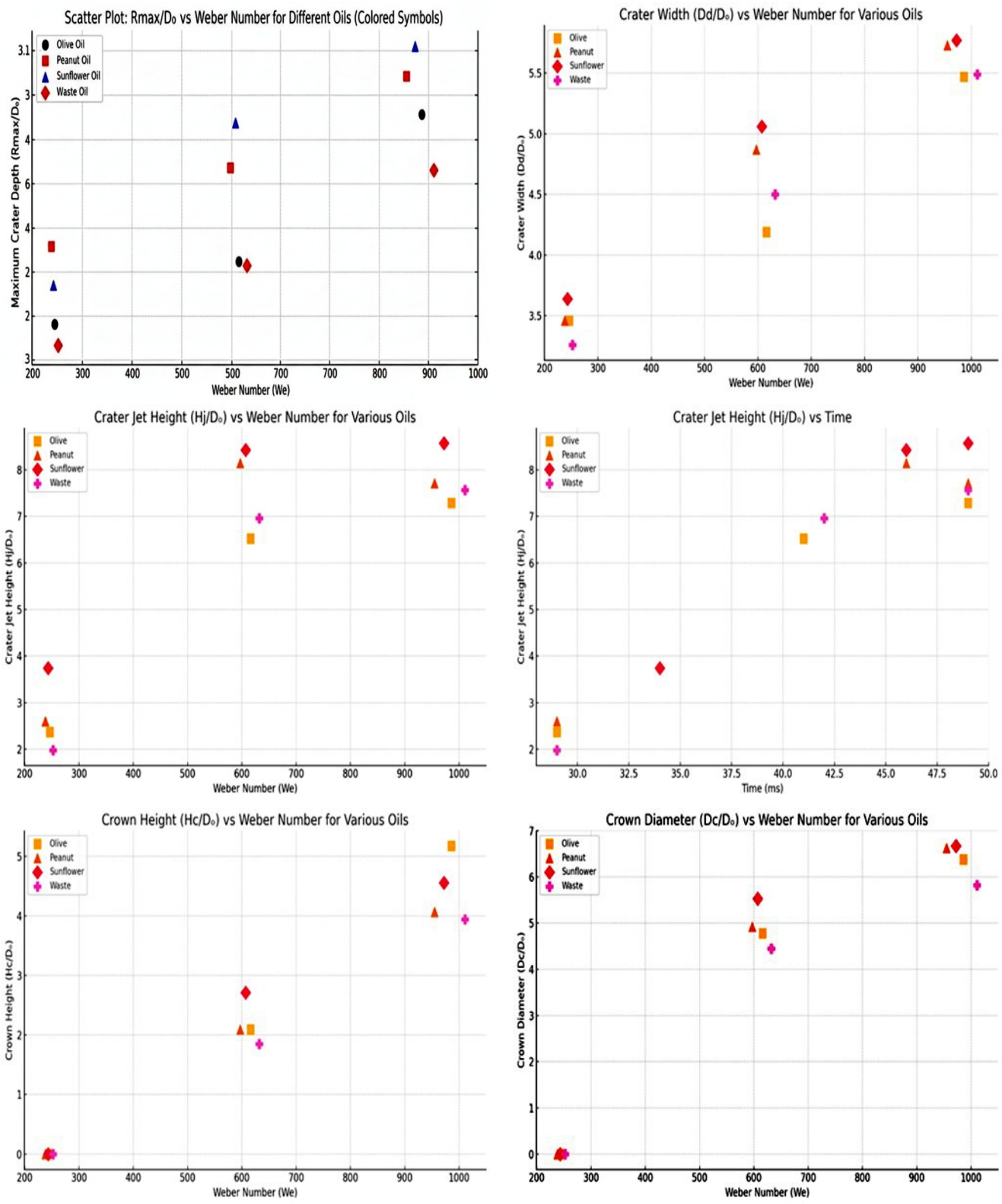

Fig. 6. Typical plots of bio-oils droplet impact on water pool surface at (RT) investigated variation of maximum non-dimensional: maximum depth R_{max} /D_oVS We, Dd/D_oVS We, H_j/D_o vs We, H_j/D_oVS Time, Hc/D_oV We, and Dc/D_o vs We

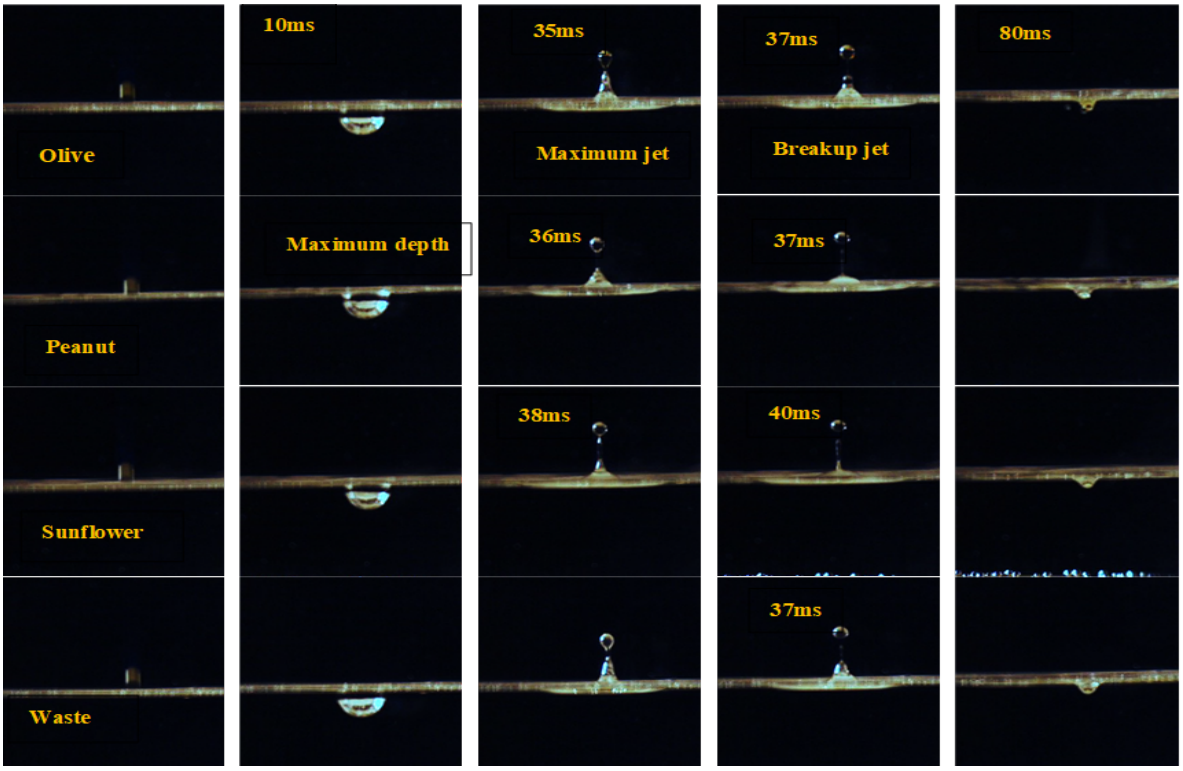

Fig. 7. Biooil single droplet on distilled water pool under 80-degree temperature with V=1.98 m/s, we number from (238 to 252), and D initial = (2.6 to 2.7 mm)

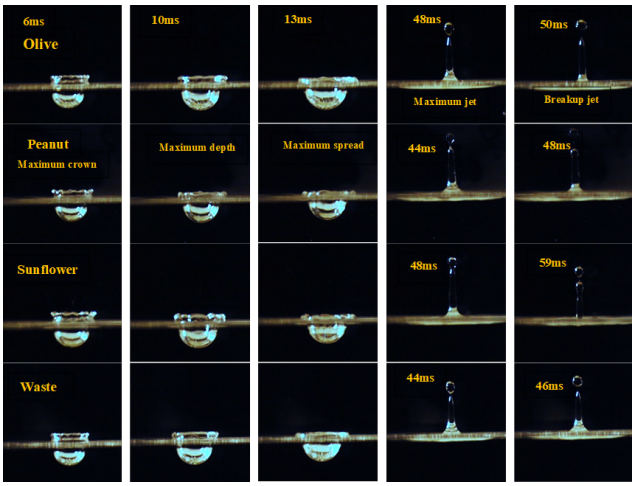

Fig. 8. Images oil droplet on distilled water pool under 80-degree temperature with V=3.13 m/s, We =616 olive, peanut 597, sunflower 607 and waste 632 and D initial = (2.6 to 2.7)

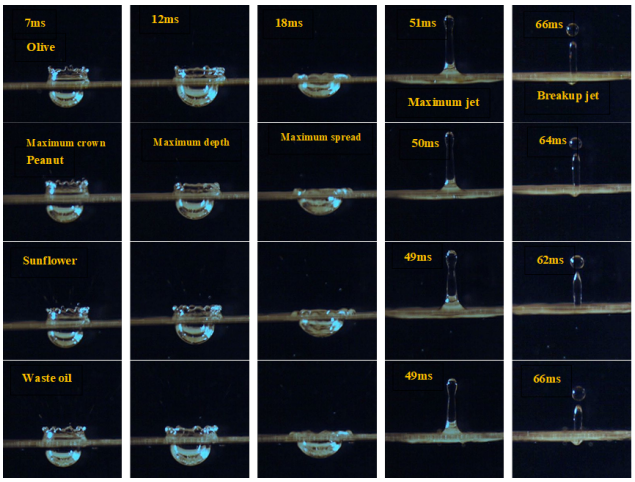

Fig. 9. Images oil droplet on distilled water pool under 80-degree temperature with V=3.96 m/s, We =986 olive, peanut 955, sunflower 972 and waste 1011 and D initial = (2.6 to 2.7)

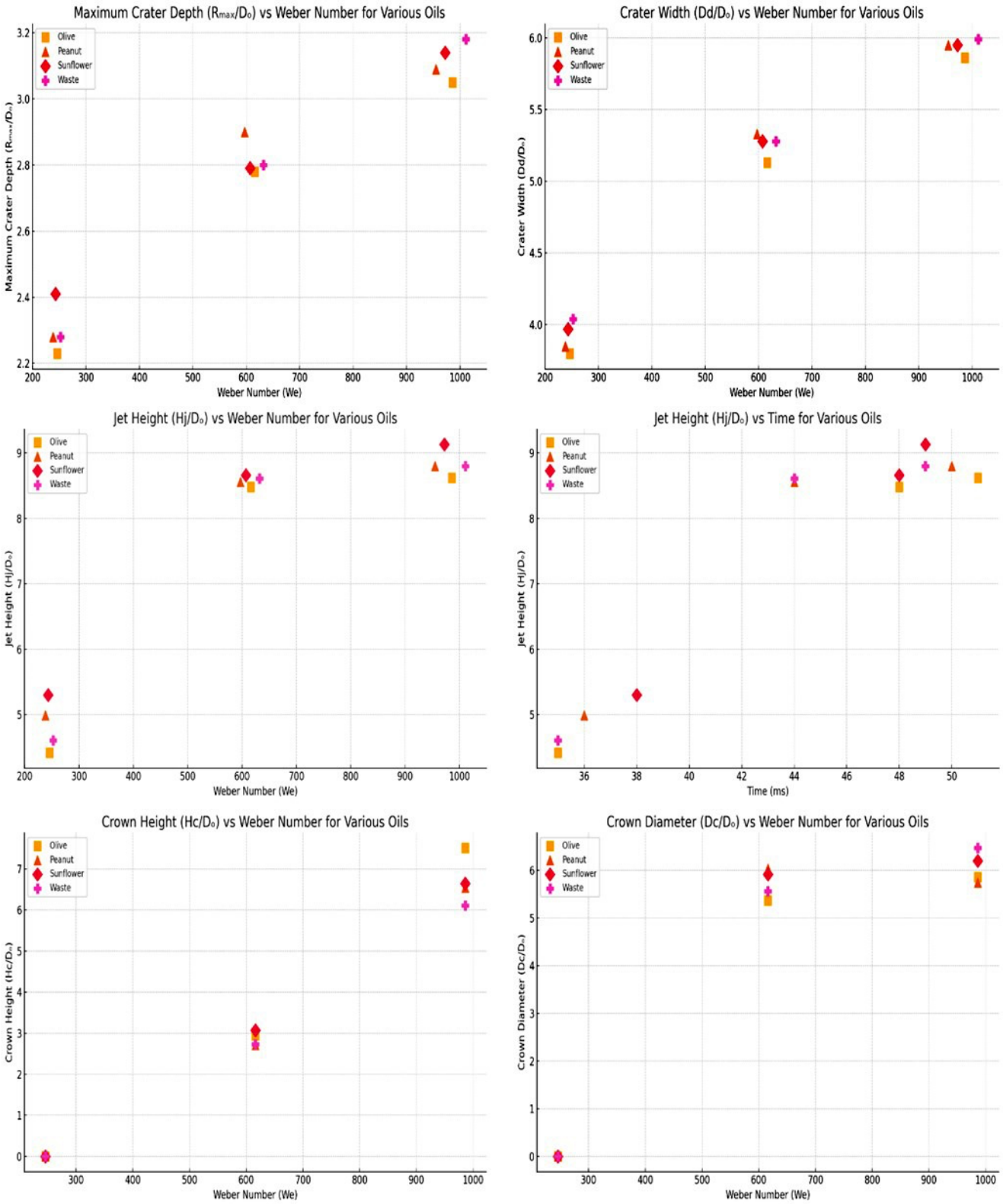

Fig. 10. Typical plots of bio-oils droplet impact on water pool surface at 80 ºC Investigated variation of maximum non-dimensional: maximum depth R_{max} /D_oVS We, Dd/D_oVS We, H_j/D_o vs We, H_j/D_oVS Time, H_c/D_oV We, and Dc/D_o vs We

3.1.2 Water-to-oil droplet impact

Compared with the oil-to-water configuration, droplets impacting oil pools show much more unstable behaviour due to the strong mismatch in viscosity and density between the two liquids. The low viscosity of water, together with the relatively viscous oil pool, promotes rapid crown growth, stronger interfacial deformation, and splash instability. As a result, water-to-oil impacts are characterized by early crown formation, rim breakup, and the ejection of secondary droplets, especially at moderate and high Weber numbers. At room temperature and low Weber number (We ≈ 172), the impact remains relatively stable because inertial forces are insufficient to generate significant interfacial instability. Shallow craters are formed ($R_{max}/D_o \approx 2.1–2.2$), and the resulting jets remain weak ($H_j/D_o \approx 1.0–2.1$), with no splashing observed (**Figure 11**). Under these conditions, the impact energy is dissipated primarily through crater formation and viscous damping within the oil pool. As the Weber number increases to the moderate regime (We ≈ 431), the impact behaviour changes substantially. Splashing begins very early, between approximately 2 and 12 ms, particularly for olive and waste oils. The crown becomes increasingly unstable, and small secondary droplets are ejected from the rim. Jet heights increase to approximately $H_j/D_o \approx 2.2–3.3$, while crown heights reach up to $H_c \approx 4.2$ (**Figure 12**). These observations show that increasing inertia amplifies interfacial instability and accelerates crown growth, while the viscosity contrast between water and oil promotes asymmetric deformation and early rim breakup. At a high Weber number (We ≈ 690), the impact enters a strongly instability-dominated regime. Large crowns are generated, reaching Hc ≈ 10.2 for olive oil, accompanied by intense splashing and multiple secondary droplets (**Figure 13**). Although jet heights increase slightly ($H_j/D_o \approx 3.6–5.2$), they remain lower than those observed in the oil-to-water configuration because a significant portion of the impact energy is dissipated through viscous deformation and crown expansion within the oil pool. The trends observed experimentally are further confirmed in **Figure 14**, where crown height increases sharply with Weber number, whereas jet height exhibits only moderate growth. This behaviour demonstrates that increasing inertia primarily enhances lateral crown instability rather than vertical jet amplification in the water-to-oil configuration. When the pool temperature is increased to 80 °C, the instability becomes substantially more pronounced (**Figures 15–17**). Splashing occurs at all Weber numbers, with crown heights significantly increasing to $H_c \approx 12.3$. In addition, a secondary jet forms after collapse of the primary cavity, appearing between approximately 104 and 121 ms (**Figure 18**). This behaviour indicates that elevated temperature reduces oil viscosity and increases interfacial mobility, thereby enhancing cavity oscillation and promoting stronger rebound dynamics. The resulting reduction in viscous resistance allows crown instability and splash formation to develop more rapidly and intensely. Overall, the water-to-oil configuration represents the most unstable impact regime investigated in this study. The combined effects of high inertia, liquid–liquid asymmetry, and increased interfacial mobility at elevated temperature promote rapid crown growth, rim breakup, and the formation of secondary droplets. These results show that the Weber number and temperature strongly intensify instability, while the viscosity difference between the two liquids controls the transition from stable crater development to splash-dominated behaviour.

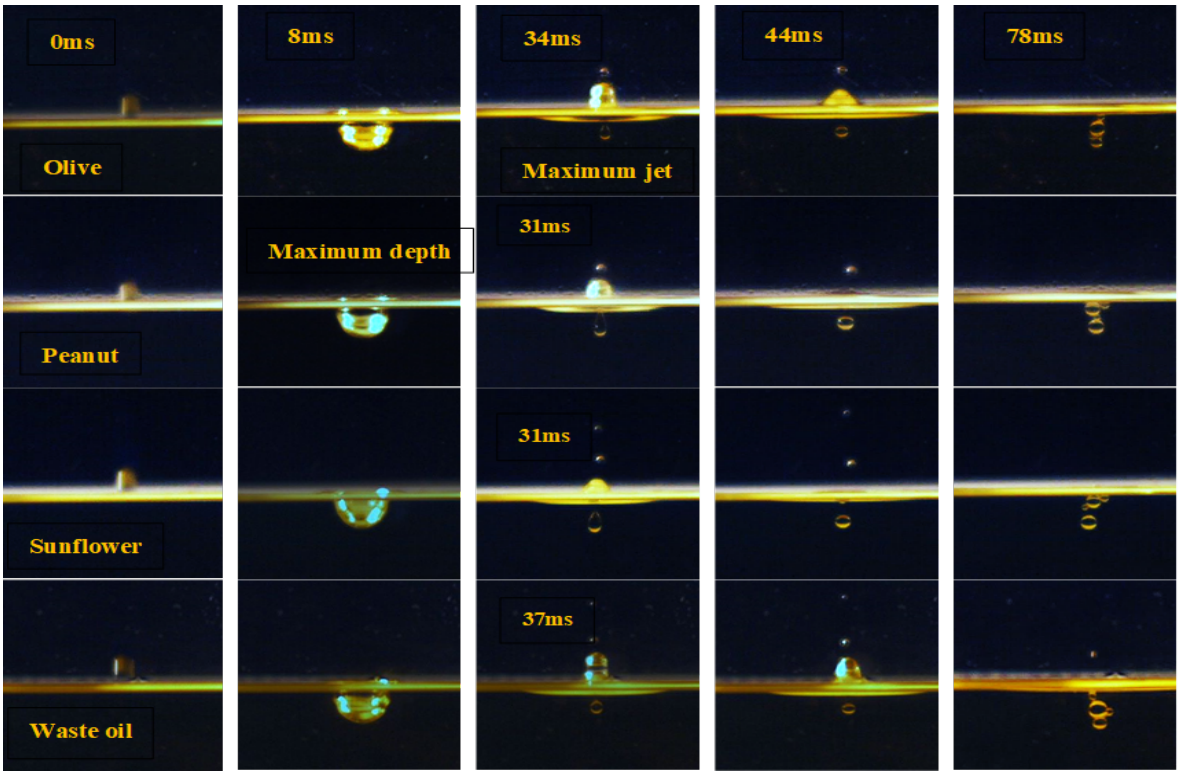

Fig. 11. Distilled water droplet on bio-oils pool under room temperature with V = 1.98 m/s, We = 172, Oh = 0.002, and Re = 6278

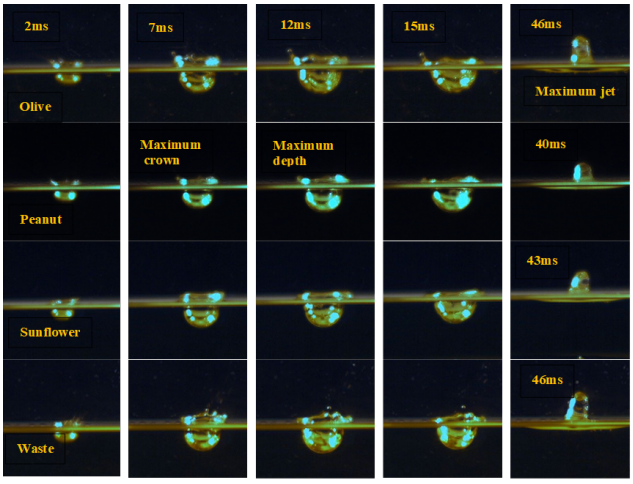

Fig. 12. Distilled water droplet on oil pool under room temperature with V=3.13 m/s, We =431, Oh = 0.002 and Re = 9924

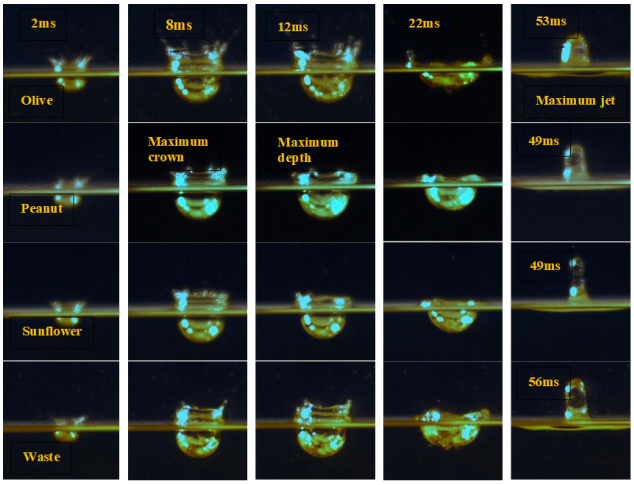

Fig. 13. Distilled water droplet on oil pool under room temperature with V=3.96 m/s, We = 690, Oh = 0.002 and Re = 12556

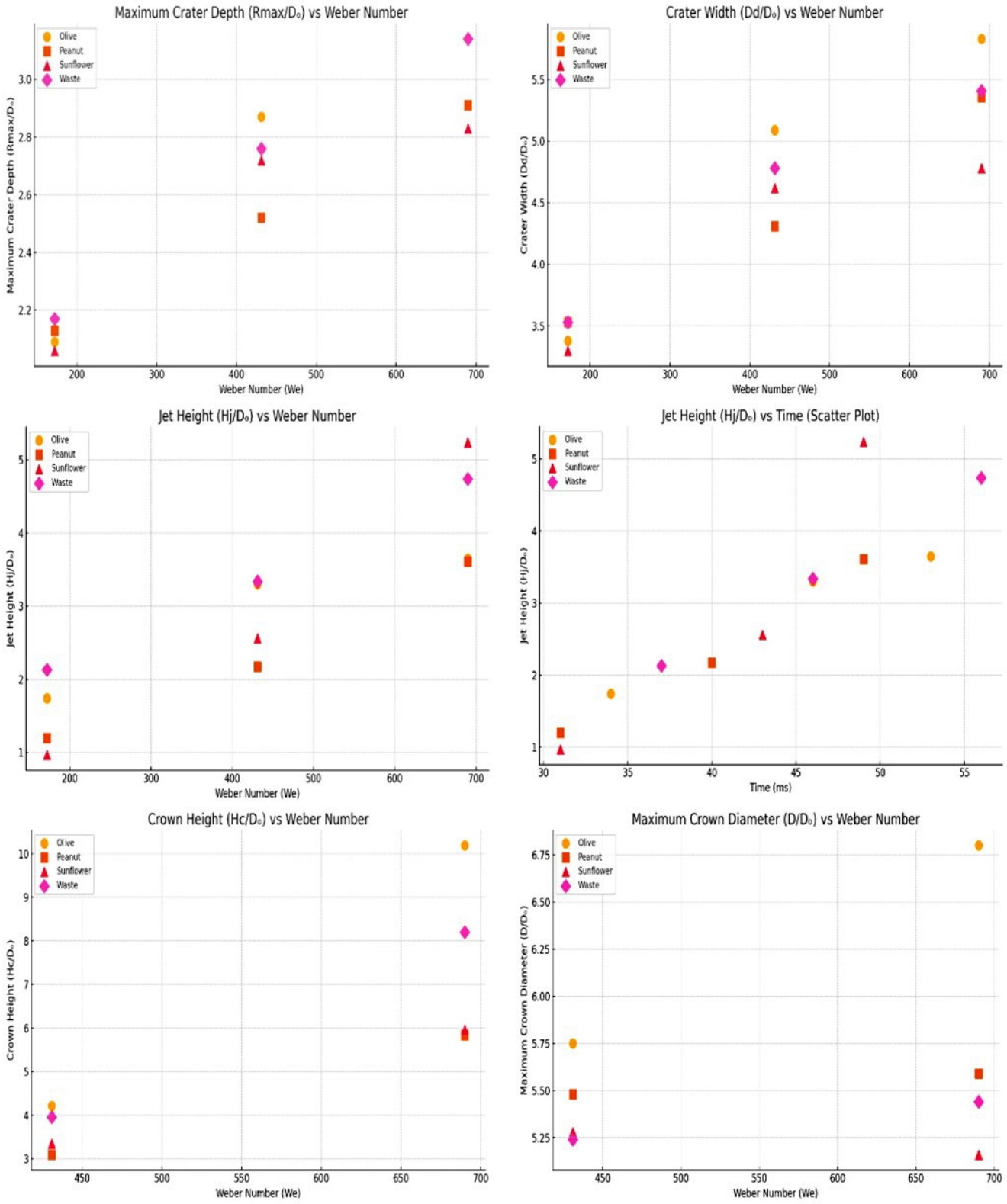

Fig. 14. Typical plots of distilled water droplet impact on bio-oils pool surface at (room temperature) investigated variation of maximum non-dimensional: R_{max} /D_oVS We, D_d/D_oVS We, H_j/D_o vs We, H_j/D_oVS Time, H_c/D_oV We, and D_c/D_o vs We

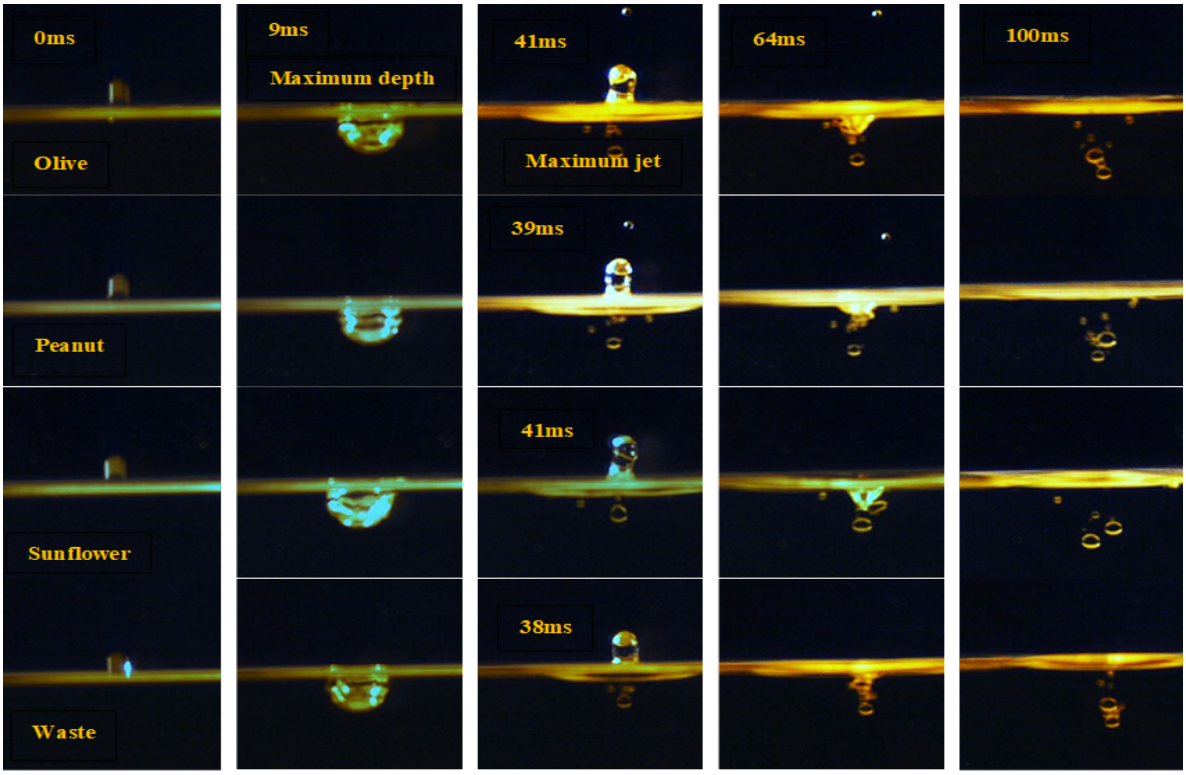

Fig. 15. Distilled water droplet on oil pool under 80-degree temperature with V= 1.98 m/s, We = 172, Oh = 0.002 and Re = 6278

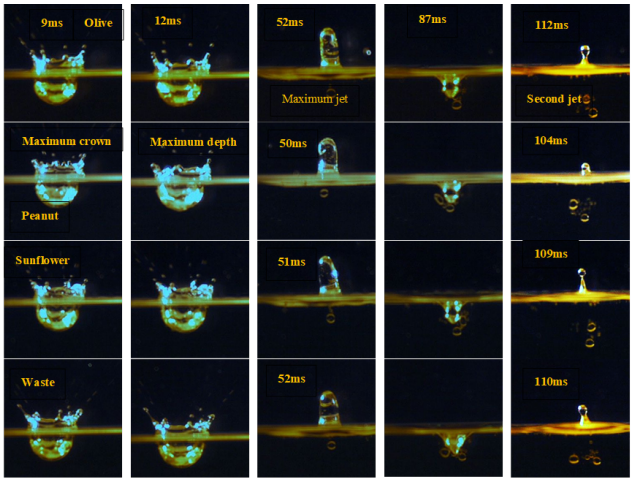

Fig. 16. Distilled water droplet on oil pool under 80-degree temperature with V=3.13 m/s, We =431, Oh = 0.002 and Re = 9924

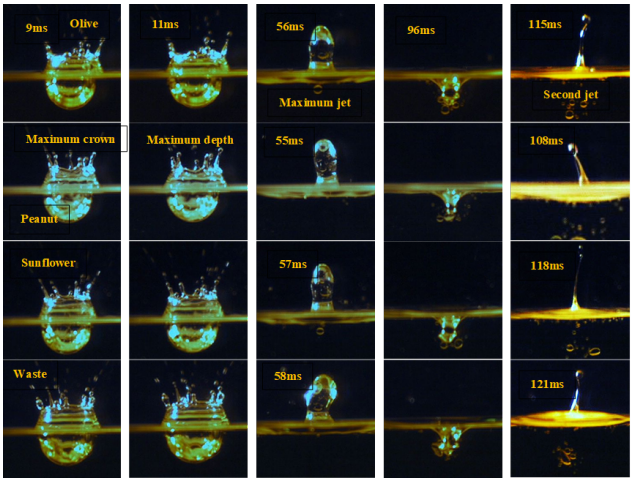

Fig. 17. Distilled water droplet on oil pool under 80-degree temperature with V=3.96 m/s, We = 690, Oh = 0.002 and Re = 12556

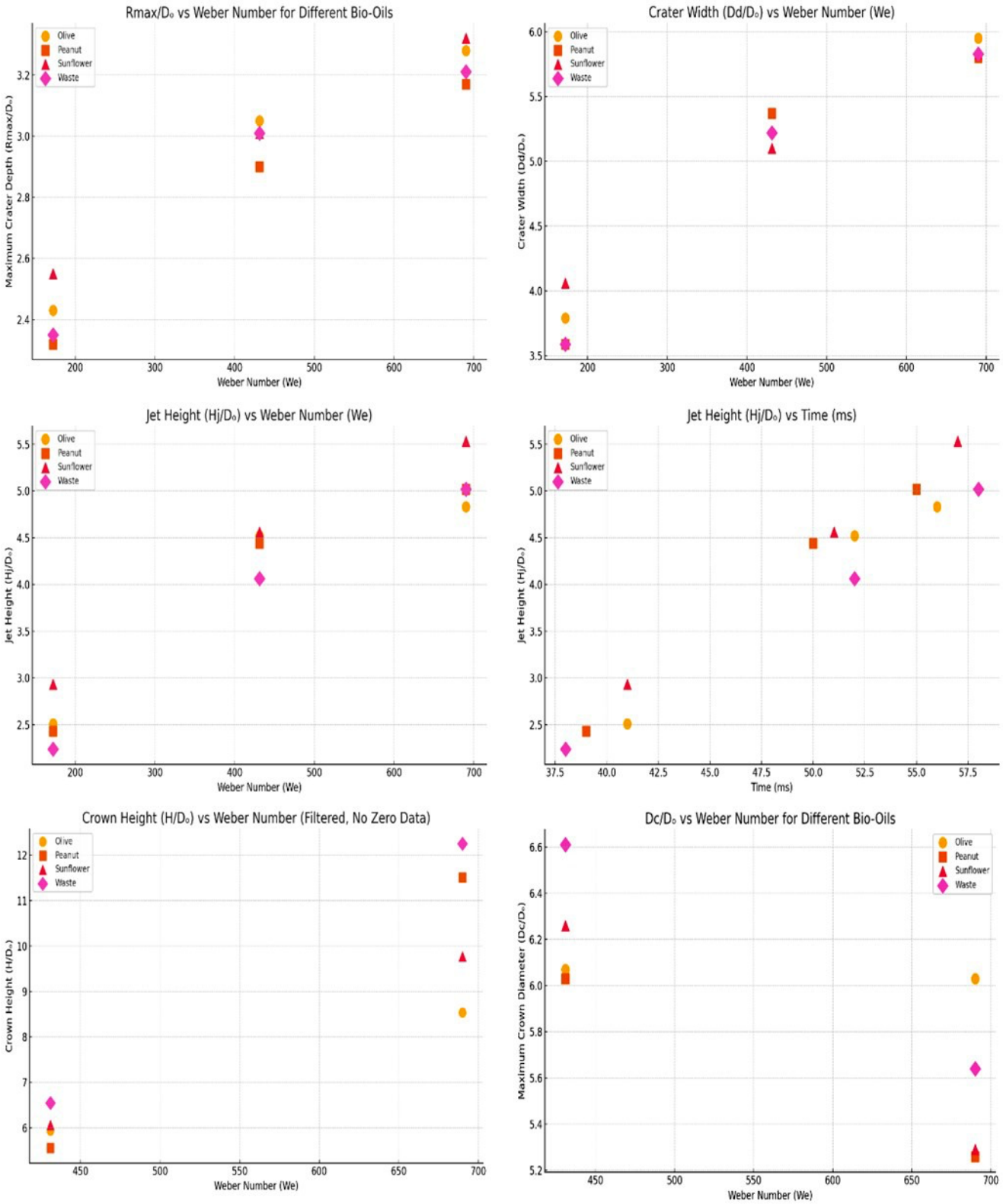

Fig. 18. Typical plots of distilled water droplet impact on bio-oils pool surface at 80 ºC Investigated variation of maximum non-dimensional: maximum depth R_{max} /D_oVS We, D_d/D_oVS We, H_j/D_o vs We, H_j/D_oVS Time, H_c/D_oV We, and D_c/D_o vs We

3.1.3 Water-to-water droplet impact

Water-to-water impacts represent a symmetric liquid–liquid system in which the droplet and pool possess nearly identical physical properties. Consequently, the impact dynamics are governed primarily by the balance between inertia and surface tension, without the strong viscosity asymmetry observed in the water-to-oil and oil-to-water configurations. This symmetry promotes relatively uniform crater evolution and efficient momentum transfer during impact. At room temperature, a small splash occurs very early following impact (approximately 2 ms), accompanied by crown expansion and strong upward jet formation. As the Weber number increases, both crater depth and crown height increase progressively, while jet formation becomes significantly more pronounced (**Figure 19**). Maximum jet heights reach $H_j/D_o \approx 8.35$ at high Weber number, indicating that the symmetric transfer of impact energy efficiently amplifies vertical jet motion. Compared with the water-to-oil configuration, the water-to-water system exhibits less severe crown breakup and reduced interfacial instability because the absence of strong viscosity contrast limits asymmetric deformation and rim destabilization. When the pool temperature is increased to 80 °C, the overall impact regime remains similar, although thermal effects enhance crown development and secondary jet formation. Crown height increases significantly, particularly at moderate and high Weber numbers, indicating that elevated temperature promotes stronger interfacial deformation and cavity oscillation. In addition, a secondary jet is observed in all cases between approximately 105 and 127 ms after collapse of the primary jet (**Figure 20**). This delayed rebound behaviour suggests that thermal reduction of viscous resistance and surface tension allows the collapsing cavity to recover more rapidly and generate stronger upward momentum during the secondary oscillation cycle. The temporal evolution presented in **Figures 21** and **22** further confirms that crater depth and primary jet height remain relatively similar at both temperatures, whereas crown height and crater width increase noticeably at 80 °C. These findings show that temperature mainly increases interfacial deformation and crown instability rather than changing the overall impact regime. In general, water-to-water impacts display a more balanced behaviour, with moderate splashing, efficient jet formation, and thermally enhanced secondary jet dynamics due to the symmetric momentum transfer within the liquid system.

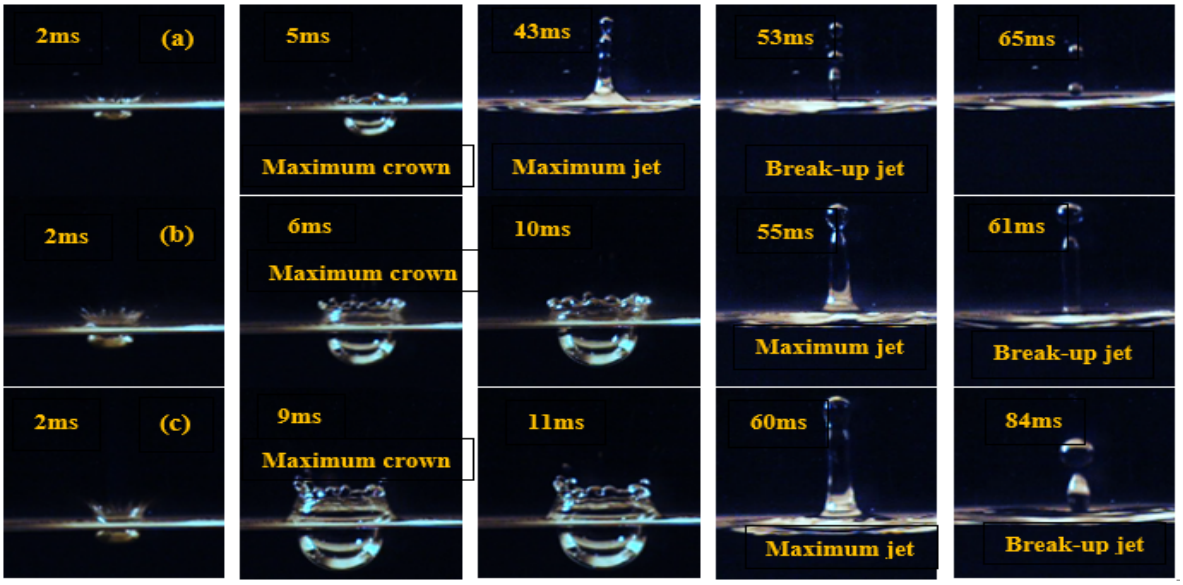

Fig. 19. Water to water under room temperature with We from (172 to 690) with velocity section (a) v = 1.98, We 172 and Fr=124 (b) v = 3.13, We 431 and Fr = 312 (c) v = 3.96, We = 690 and Fr =499 droplet diameter = 3.2 mm

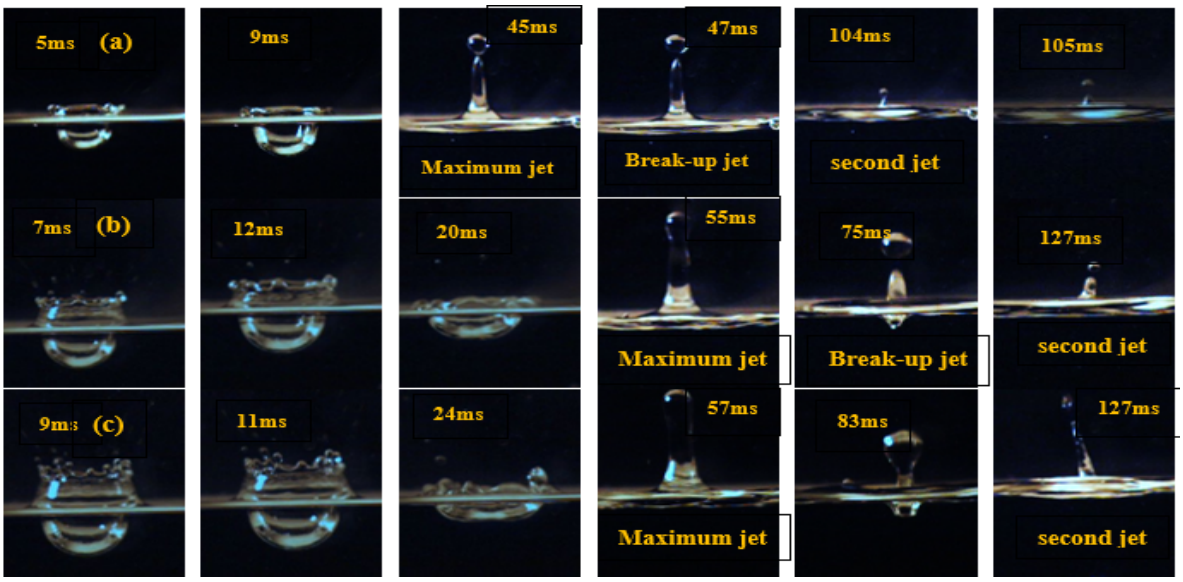

Fig. 20. Water to water under 80-degree temperature pool surface with We from (172 to 690) with velocity section (a) v = 1.98, We 172, Fr=124 (b) v = 3.13, We 431 and Fr =312 (c) v = 3.96, We = 690 and Fr =499 droplet diameter =3.2mm

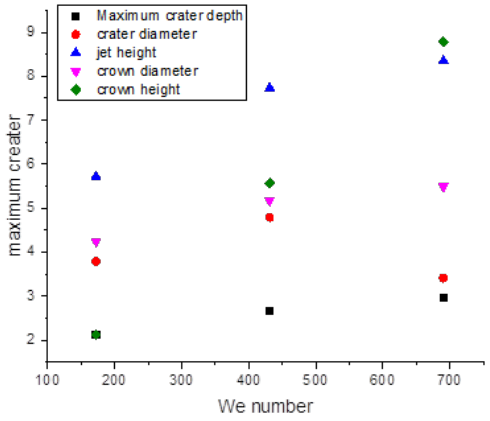

Fig. 21. Typical plots of distilled water droplet impact on water pool surface at (RT) investigated Variation of maximum non-dimensional: R_{max} /D_oVS We, D_d/D_oVS We, H_j/D_o vs We, H_c/D_oV We, and D_c/D_o vs We under three We 172, 431 and 690

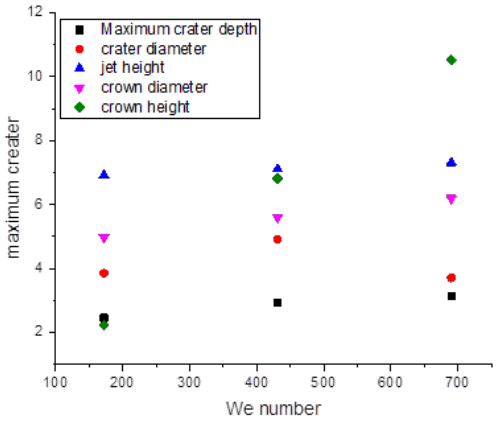

Fig. 22. Typical plots of distilled water droplet impact on water pool surface at (80 ºC) investigated variation of maximum non-dimensional: R_{max} /D_oVS We, D_d/D_oVS We, H_j/D_o vs We, H_c/D_oV We, and D_c/D_o vs We under three We 172, 431, and 690

3.1.4 Vapour explosion at 290 °C

At 290 °C, the impact of water droplets on bio-oil pools generates vapour explosion phenomena driven by rapid vapour formation beneath the impacting droplet. The onset and intensity of these explosions are governed by the coupled interaction of thermal effects, inertial penetration, and liquid viscosity. Increasing Weber number significantly accelerates instability development by enhancing droplet penetration and interfacial heat transfer, whereas higher oil viscosity delays vapour accumulation and suppresses rapid rupture. A general comparison of explosion initiation times is

presented in **Figure 23**, where increasing the Weber number consistently reduces the delay time and promotes earlier vapour explosion. For olive oil at a low Weber number (We = 172), the explosion process exhibits a relatively long delay before instability onset. The first vapour explosion occurs at approximately 258 ms, followed by subsequent events at 277, 310, 390, and 503 ms. This delayed response is associated with the relatively high viscosity of olive oil, which slows thermal transport and delays vapour accumulation beneath the droplet. As shown in **Figure 24**, the explosion develops gradually, producing moderate jetting and limited crown expansion during the early stages. When the Weber number increases to We = 690, the behaviour changes significantly. The first explosion occurs much earlier at approximately 105 ms, followed by multiple secondary events, indicating intensified instability and stronger vapour-driven fragmentation. This transition demonstrates that increased inertial penetration enhances liquid–liquid contact and accelerates vapour generation beneath the interface. Peanut oil exhibits an earlier explosion onset than olive oil at a low Weber number, with the first event occurring at approximately 165 ms, followed by successive explosions at 284, 372, 492, and 528 ms. The relatively lower viscosity of peanut oil allows more efficient energy transfer and faster vapour formation, resulting in stronger upward jetting and localized splashing (**Figure 25**). At high Weber numbers, peanut oil displays both early and delayed instability cycles, with explosion events occurring at approximately 116, 255, 797, 905, and 1097 ms. These repeated events indicate that strong inertial penetration initiates early vapour rupture, while subsequent cavity oscillation and residual thermal energy sustain delayed secondary boiling cycles. Sunflower oil exhibits the most delayed explosion response at a low Weber number. The first explosion occurs at approximately 458 ms, followed by additional events at 597, 614, 855, and 1011 ms. This delayed onset indicates that the droplet spreads more stably before vapour rupture occurs, allowing gradual energy accumulation within the liquid layer. As illustrated in **Figure 26**, the explosion initially remains moderate but becomes increasingly intense during later stages as jetting and crown collapse amplify interfacial instability. At high Weber numbers, the explosion timing is drastically reduced, with the first event occurring as early as 66ms, confirming the dominant role of inertia in accelerating vapour rupture and instability growth. For waste oil, the explosion process at low Weber number begins at approximately 252 ms, followed by several closely spaced events at 366, 375, 397, and 416 ms. Compared with the other oils, the explosions remain relatively damped, producing smaller jets and more controlled deformation due to the higher effective viscosity of the waste-oil mixture (**Figure 27**). However, at a high Weber number, waste oil exhibits the earliest explosion onset among all tested oils, with the first event occurring at only 14 ms. Under these conditions, inertial forces strongly dominate over viscous resistance, resulting in highly violent fragmentation and chaotic jetting immediately after impact. Overall, the vapour explosion behaviour is governed by the competition between thermal vapour generation, inertial penetration, and viscous damping. At a low Weber number, heat transfer and vapour accumulation dominate the process, resulting in delayed and relatively controlled explosions. In contrast, at a high Weber number, enhanced inertial penetration intensifies interfacial contact and accelerates vapour rupture, producing earlier and more violent explosions. These findings demonstrate that temperature alone does not determine explosion severity; rather, the coupled effects of Weber number, viscosity, and thermal interaction collectively control the transition from delayed boiling to explosive fragmentation. The quantitative trends of explosion timing and instability development are summarized in **Table 3**.

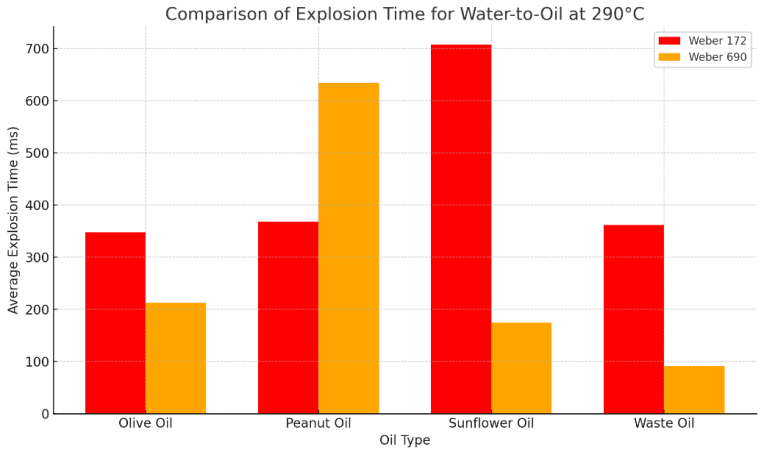

Fig. 23. Explosion times of distilled water droplets impacting bio-oil pools at 290 °C

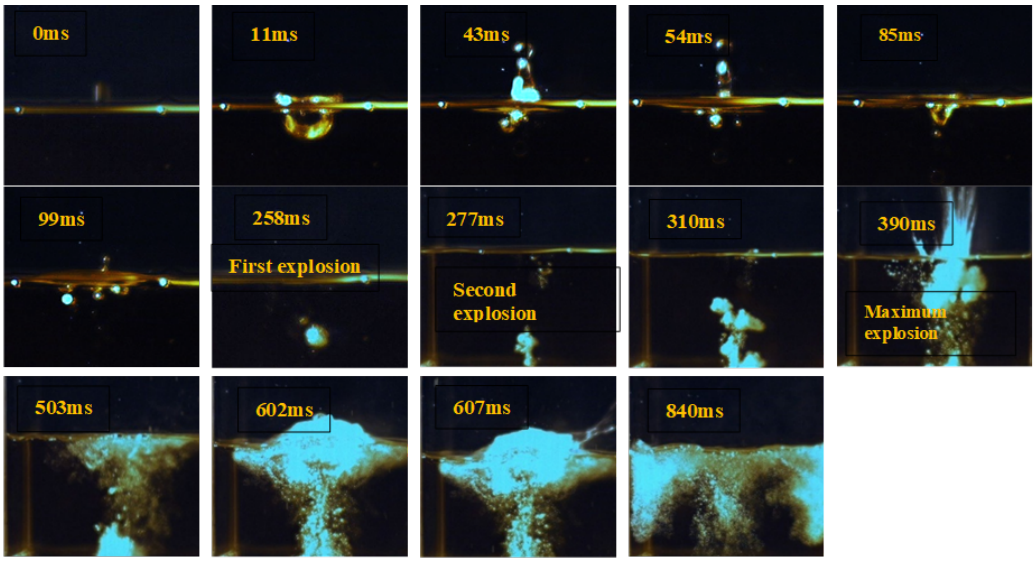

Fig. 24. Full dynamic process time of vapor explosions of distilled water droplet impact on olive oil pool surface (We = 172, T_{oil} = 290 ◦C & diameter =3.2 mm)

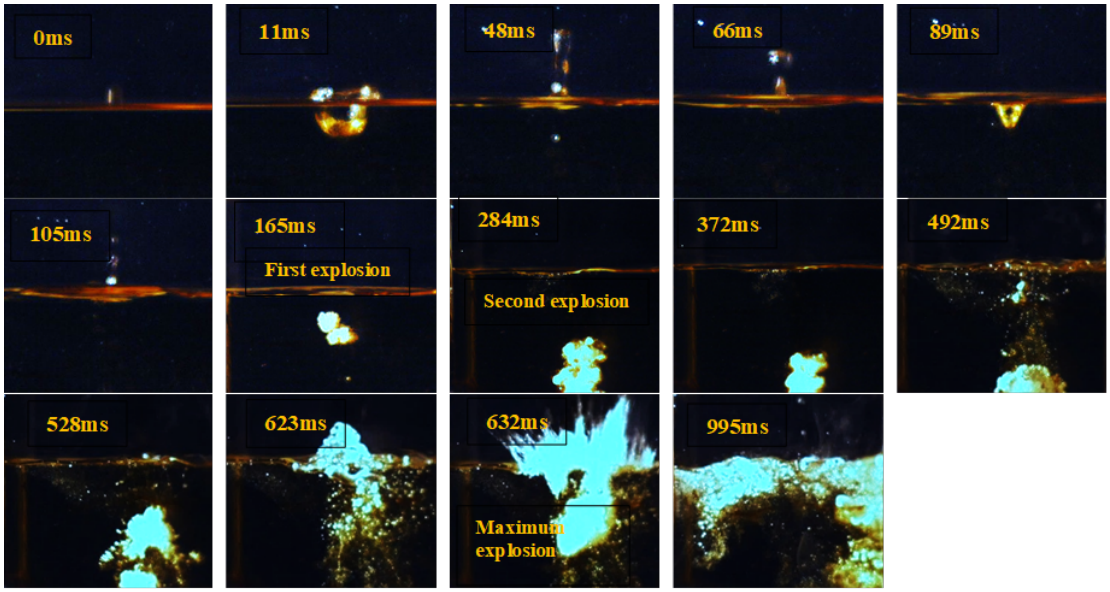

Fig. 25. Full dynamic process time of vapor explosions of distilled water droplet impact on peanut oil pool surface (We =172, T_{oil} = 290 ◦C & diameter =3.2 mm)

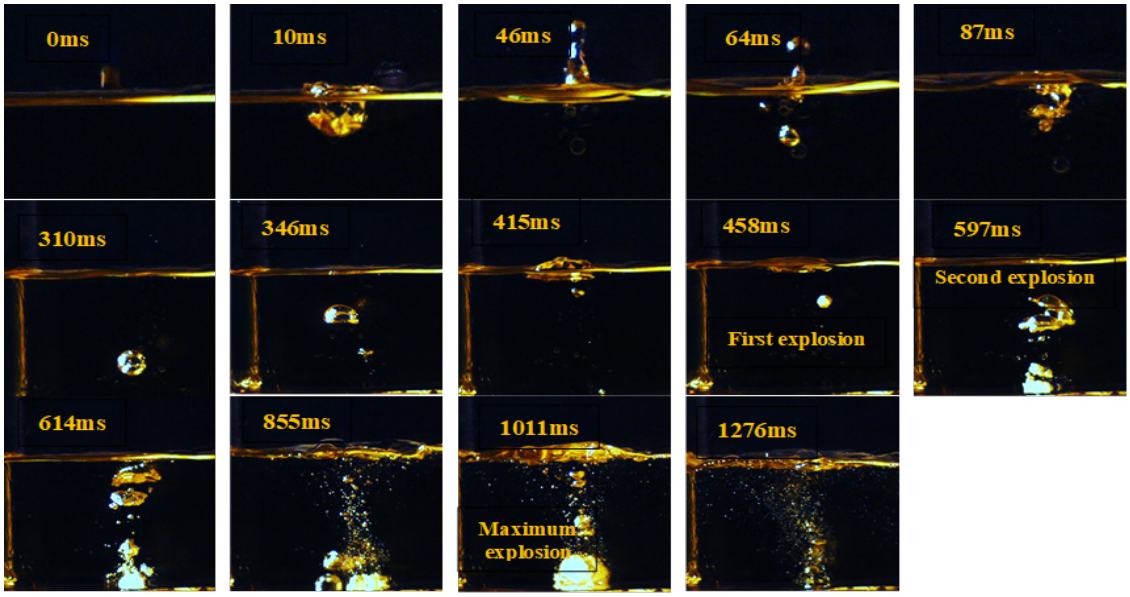

Fig. 26. Full dynamic process time of vapor explosions of distilled water droplet impact on sunflower oil pool surface (We = 172, T_{oil} = 290 ◦C & diameter =3.2 mm)

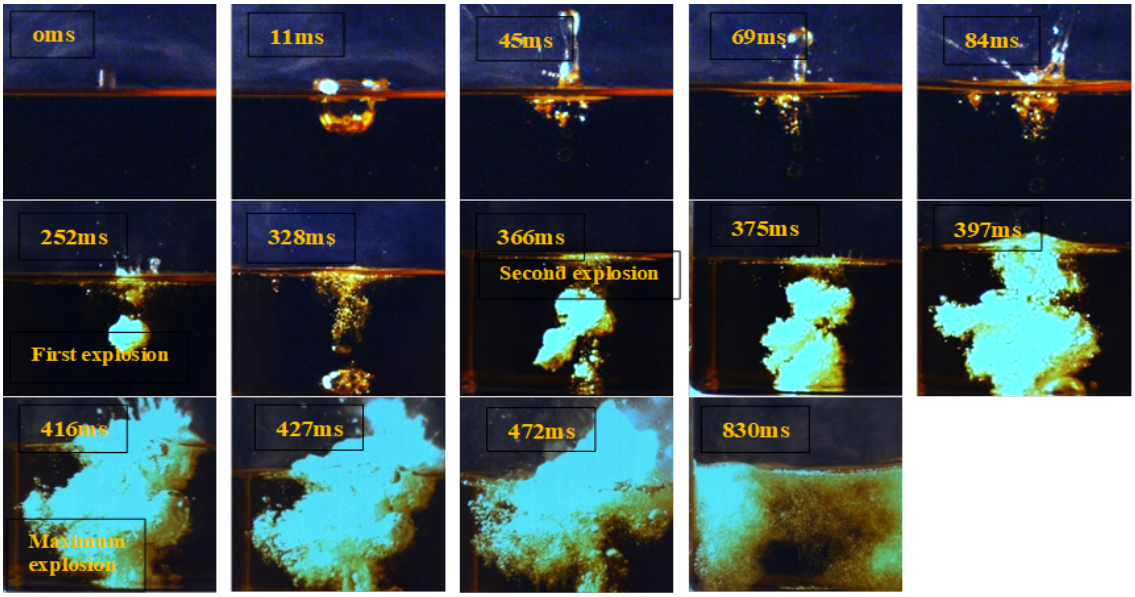

Fig. 27. Full dynamic process time of vapor explosions of distilled water droplet impact on WCOO pool surface (We of water = 172, T_{oil} = 290 ºC & diameter =3.2 mm)

Table 3
Explosion time ranges for water-to-oil droplet impacts at 290 °C

Weber number	Explosion time (olive oil)	Explosion TIME (peanut oil)	Explosion TIME (sunflower oil)	Explosion TIME (WCOO)
172	258	165	458	252
172	277	284	597	366
172	310	372	614	375
172	390	492	855	397
172	503	528	1011	416
690	105	116	66	14
690	132	255	77	38
690	174	797	113	61
690	302	905	284	83
690	350	1097	333	260

3.1.5 Key findings across all cases

To provide an overall interpretation of the experimental results, the jet breakup behaviour for all investigated liquid–liquid interaction configurations is summarized in Table 4. The results show that jet stability and breakup are controlled mainly by the combined effects of Weber number, temperature, viscosity, and liquid configuration. In general, increasing Weber number enhances jet instability by strengthening inertial penetration and cavity collapse, whereas higher viscosity suppresses breakup through greater energy dissipation. Increasing temperature further modifies the behaviour by reducing viscous resistance and enhancing interfacial motion. At room temperature (28°C), the breakup behaviour strongly depends on both impact configuration and Weber number. In the oil-to-water configuration, no jet breakup is observed at low impact velocity (V_1 = 1.98 m/s), indicating that inertial forces are insufficient to overcome viscous damping and surface tension effects. As the impact velocity increases (V_2 and V_3), jet breakup becomes more noticeable, reflecting

the increasing influence of inertia on jet destabilization. In contrast, the water-to-oil configuration shows the opposite trend. Jet breakup occurs at low velocity but becomes less pronounced at higher velocities. This behaviour is attributed to the relatively high viscosity of the oil pool, which absorbs a significant portion of the impact energy and stabilizes the jet despite the increase in inertia. For the water-to-water configuration, jet breakup is observed at all velocities. Because both liquids have similar physical properties, cavity collapse and jet formation occur more efficiently, leading to repeated jet instability and breakup events. At elevated temperatures (80 °C), the breakup behaviour changes significantly due to reduced viscosity and increased interfacial mobility. In the oil-to-water configuration, jet breakup is observed at all velocities, indicating that heating weakens viscous stabilization and allows instability to develop even at relatively low Weber numbers. The water-to-oil configuration exhibits more complex behaviour. At low velocity, no breakup is observed, suggesting that thermal effects alone are insufficient to overcome viscous damping. At moderate velocity, limited breakup appears, particularly for sunflower oil, indicating partial destabilization of the jet. At high velocity, however, all cases exhibit breakup, often after the formation of a secondary jet. This behaviour highlights the combined influence of inertia and temperature in promoting delayed instability and repeated jet fragmentation. For the water-to-water configuration at 80 °C, multiple breakup events are observed. Two successive breakup events frequently occur at low and moderate velocities, corresponding to the primary and secondary jets formed during cavity collapse and rebound. At high velocity, breakup occurs mainly during the secondary jet stage, indicating that elevated temperature enhances cavity oscillation and promotes repeated jet formation. These observations confirm that heating intensifies interfacial instability without fundamentally changing the overall impact behaviour. At the highest temperature investigated (290°C), the impact behaviour transitions from conventional jetting and crown dynamics to a vapour-explosion regime. Under these conditions, the interaction is governed by the combined effects of thermal energy, inertial penetration, and liquid viscosity. Increasing the Weber number accelerates vapour rupture and significantly reduces the explosion delay time by enhancing droplet penetration and interfacial heat transfer. In contrast, higher-viscosity oils tend to delay instability development and moderate the intensity of fragmentation by suppressing rapid vapour expansion. These observations indicate that thermal effects become increasingly dominant at elevated temperatures, producing impact regimes that differ fundamentally from those observed at 28 °C and 80 °C. Overall, the impact and breakup behaviour observed across all configurations is governed by the coupled interactions of inertia, viscosity, temperature, and liquid configuration. Increasing Weber number promotes crater growth, crown instability, jet breakup, and fragmentation, whereas higher viscosity suppresses instability through enhanced energy dissipation. Temperature reduces viscous resistance, increases interfacial mobility, and, at sufficiently high values, can trigger vapour-explosion phenomena. Among the investigated configurations, the water-to-oil system exhibits the strongest instability due to the large difference in liquid properties, whereas the oil-to-water configuration remains comparatively stable because of viscous damping and liquid-pool cushioning. The water-to-water configuration represents an intermediate regime characterized by efficient cavity collapse and repeated jet formation. These findings provide useful guidance for controlling jet instability, splash formation, and vapour-explosion behaviour in applications such as fuel atomization, spray cooling, thermal management, and renewable-fuel systems, where operating temperature and impact conditions strongly influence droplet stability, heat transfer performance, and process safety.

Table 4
Jet breakup behavior of bio-oil and water droplets at different impact velocities and temperatures across various liquid–Liquid interaction scenarios

case	T	Low We	Moderate We	High We	T	Low We	Moderate We	High We
Oil to water	28 ◦C →	No jet breakup	Jet Breakup	Jet Breakup	80 ◦C →	Jet Breakup	Jet Breakup	Jet Breakup
Water to oil	28 ◦C →	Jet Breakup	No jet breakup	No jet breakup	80 ◦C →	No jet breakup	Just sunflower breakup	All jets break after the second jet
Water to water	28 ◦C →	Jet Breakup	Jet Breakup	Jet breakup	80 ◦C →	Breakup two times with one and second jet	Breakup two times with one and second jet	Breakup one time with a second jet

4. Conclusions

This study experimentally investigated the impact behaviour of bio-oil and water droplets on shallow liquid pool surfaces under different Weber numbers and thermal conditions for oil-to-water, water-to-oil, and water-to-water configurations. The results show that droplet impact dynamics are controlled by the combined effects of inertia, viscosity, temperature, and liquid–liquid interaction. Increasing Weber number enhances crater deformation, crown growth, jet instability, and fragmentation, whereas higher liquid viscosity suppresses instability through viscous damping and energy dissipation. Increasing temperature further intensifies interfacial deformation and vapour generation by reducing viscous resistance and increasing liquid mobility. Among the investigated configurations, the oil-to-water case remained the most stable under all tested conditions. The combined effects of bio-oil viscosity and liquid-pool cushioning suppressed splashing and maintained relatively stable jet development. In contrast, the water-to-oil configuration exhibited the strongest instability, where the large viscosity difference between water and oil promoted rapid crown breakup, secondary droplet formation, and enhanced jet fragmentation, particularly at elevated temperatures. The water-to-water configuration showed more balanced behaviour, with efficient cavity collapse, repeated jet formation, and moderate breakup due to the similar physical properties of the interacting liquids. At 290 °C, the impact process transitioned into a vapour explosion regime controlled by the interaction between thermal effects, inertial penetration, and viscous resistance. Higher Weber number accelerated vapour rupture and intensified fragmentation, while higher-viscosity oils delayed instability development and reduced explosion severity. These observations demonstrate that vapour explosion behaviour is not controlled by temperature alone but by the coupled effects of inertia, viscosity, and thermal interaction. Overall, the present findings provide a clearer physical understanding of droplet–liquid interactions involving bio-oils over a wide range of thermal and dynamic conditions. The results also provide useful guidance for controlling splash formation, jet instability, and vapour explosion behaviour in applications such as spray cooling, fuel atomization, thermal management, and renewable fuel systems. In particular, the findings suggest that operating temperature, impact conditions, and liquid viscosity can be adjusted to improve droplet stability, reduce unwanted fragmentation, and enhance process safety in high-temperature applications. The present study is limited to shallow pool conditions, a specific Weber number range, and selected bio-oil formulations. Future work should investigate deeper liquid pools, wider thermal

conditions, and additional fuel compositions to further understand the relationship between interfacial heat transfer, vapour instability, and droplet fragmentation dynamics.

Acknowledgement
This research was supported by Ministry of Higher Education Malaysia under the Fundamental Research Grant Scheme (FRGS/1/2020/TK0/USM/03/10), and this support is gratefully acknowledged.

References

[1] Liang, Gangtao, Yong Yang, Yali Guo, Ni Zhen, and Shengqiang Shen. "Rebound and spreading during a drop impact on wetted cylinders." *Experimental thermal and fluid science* 52 (2014): 97-103. https://doi.org/10.1016/j.expthermflusci.2013.09.001

[2] Thoroddsen, Sigurdur T., Takeharu Goji Etoh, and Kohsei Takehara. "High-speed imaging of drops and bubbles." *Annu. Rev. Fluid Mech.* 40, no. 1 (2008): 257-285. https://doi.org/10.1146/annurev.fluid.40.111406.102215

[3] Yarin, Alexander L. "Drop impact dynamics: Splashing, spreading, receding, bouncing…." *Annu. Rev. Fluid Mech.* 38, no. 1 (2006): 159-192. https://doi.org/10.1146/annurev.fluid.38.050304.092144

[4] Mohammad Karim, Alireza. "Physics of droplet impact on various substrates and its current advancements in interfacial science: A review." *Journal of Applied Physics* 133, no. 3 (2023). https://doi.org/10.1063/5.0130043

[5] Mohammad Karim, Alireza. "Physics of droplet impact on flexible materials: A review." *Advances in Mechanical Engineering* 14, no. 11 (2022): 16878132221137237. https://doi.org/10.1177/16878132221137237

[6] Wang, Xin, Bo Xu, Shuai Guo, Yu Zhao, and Zhenqian Chen. "Droplet impacting dynamics: Recent progress and future aspects." *Advances in Colloid and Interface Science* 317 (2023): 102919. https://doi.org/10.1016/j.cis.2023.102919

[7] Josserand, Christophe, and Sigurdur T. Thoroddsen. "Drop impact on a solid surface." *Annual review of fluid mechanics* 48, no. 1 (2016): 365-391. https://doi.org/10.1146/annurev-fluid-122414-034401

[8] Che, Zhizhao, and Omar K. Matar. "Impact of droplets on immiscible liquid films." *Soft Matter* 14, no. 9 (2018): 1540-1551. https://doi.org/10.1039/C7SM02089A

[9] Purvis, Richard, and F. T. Smith. "Droplet impact on water layers: post-impact analysis and computations." *Philosophical Transactions of the Royal Society A: Mathematical, Physical and Engineering Sciences* 363, no. 1830 (2005): 1209-1221. https://doi.org/10.1098/rsta.2005.1562

[10] Tian, Shu, and Atena Ghaderi. "Numerical investigation of water droplet collision dynamics on moving surfaces." *Scientific Reports* 15, no. 1 (2025): 4629. https://doi.org/10.1038/s41598-025-87937-1

[11] Fan, Xujun, Changjian Wang, Fangpeng Guo, Bing Chen, and Manhou Li. "Water droplet impact on high-temperature peanut oil surface: The effects of droplet diameter and oil temperature." *International Journal of Thermal Sciences* 159 (2021): 106601. https://doi.org/10.1016/j.ijthermalsci.2020.106601

[12] Manzello, Samuel L., Jiann C. Yang, and Thomas G. Cleary. "On the interaction of a liquid droplet with a pool of hot cooking oil." *Fire safety journal* 38, no. 7 (2003): 651-659. https://doi.org/10.1016/S0379-7112(03)00048-1

[13] Fan, Xujun, Changjian Wang, and Fangpeng Guo. "Experimental study of flame expansion induced by water droplet impact on the burning cooking oil." *Fuel* 270 (2020): 117497. https://doi.org/10.1016/j.fuel.2020.117497

[14] Fan, Xujun, Changjian Wang, Manhou Li, Bing Chen, Xing Wang, and Aifeng Zhang. "Dynamic behavior of single droplet impacting on heptane pool with different depths." *European Journal of Mechanics-B/Fluids* 72 (2018): 144-151. https://doi.org/10.1016/j.euromechflu.2018.05.009

[15] Xu, MingJun, JiaQing Zhang, Quan Li, and ShouXiang Lu. "The influence of liquid pool temperature on the critical impact Weber number for surface bubble formation." *International Journal of Heat and Mass Transfer* 127 (2018): 677-682. https://doi.org/10.1016/j.ijheatmasstransfer.2018.08.085

[16] Xu, MingJun, JiaQing Zhang, ChaoPeng Wu, ChangHai Li, Xiao Chen, and ShouXiang Lu. "Collision dynamics of a single water droplet impinging on a high-temperature pool of oil." *Acta Mechanica* 229, no. 4 (2018): 1567-1577.https://doi.org/10.1007/s00707-017-2071-5

[17] Wang, Zhigang, Xishi Wang, Pei Zhu, Pingping Chen, Xiangdi Zhao, and Heping Zhang. "Experimental study on the vapor explosion process of a water drop impact upon hot molten-ghee surface." *Journal of Loss Prevention in the Process Industries* 49 (2017): 839-844. https://doi.org/10.1016/j.jlp.2017.03.013

[18] Moon, Joo Hyun, Minhaeng Cho, and Seong Hyuk Lee. "Dynamic wetting and heat transfer characteristics of a liquid droplet impinging on heated textured surfaces." *International Journal of Heat and Mass Transfer* 97 (2016): 308-317. https://doi.org/10.1016/j.ijheatmasstransfer.2016.02.041

[19] Chen, Desheng, Wenhao Sun, Caihua Zhou, Xuejin Zhu, Aoqi Feng, and Zhe Lin. "Influence of droplet parameters on the dynamic characteristics of droplet collision with a moving wall surface." *Chemical Engineering Science* (2025): 122409. https://doi.org/10.1016/j.ces.2025.122409